Niobium surface defect induced by strong electric field probed by soft x-ray laser interferometry

F. Albert[a], Ph . Zeitoun[a], D. Joyeux[b], M. Boussoukaya[ac], A. Carillon[a], S. Hubert[a], P. Jaeglé[a], G. Jamelot[a], A. Klisnick[a], D. Phalippou[b], D. Ros[a], S. Sebban[a] and A. Zeitoun-Fakiris[c]

[a]LSAI, Batiment 350, Université Paris-Sud, 91 405 ORSAY Cedex, France
[b]IOTA, Batiment 503, Université Paris-Sud, 91 405 ORSAY Cedex, France.
[c]CEA-DSM, DAPNIA, SEA, CEN Saclay,91 191 Gif sur Yvette Cedex, France

ABSTRACT

Using a recent technique of X-ray laser interferometry we performed the first 'in situ' probe of defects induced on niobium surface by strong electric field. For the first time the modification of Nb surface state was observed during the growth of the electric field. The X-ray laser emits bright, 80ps-duration pulses at $\lambda = 21.2$ nm. The beam is reflected on the niobium surface under grazing incidence in a vacuum chamber. The interferometer is of the wave-front division type. Interferograms are single shot recorded, which affords us to probe 'instantaneous' defect morphology. We observed the appearance and the evolution of defects between 14 MV/m and 35 MV/m. The vertical set amplitude is of 100-200 Å. The observed position of a surface perturbed zone proved to be shifted by 500 μm under constant electric field (35 MV/m) between the instants of two laser shots (20 mn time interval).

Keywords: soft x-ray laser, X-W interferometry, surface defect analysis, niobium, strong electric field, superconductive cavities.

I. INTRODUCTION.

X-ray lasers have already been used for applications in plasma physics [1] and solid state physics on fluorescence of ionic crystals[2]. At LULI[3] the first demonstration of x-ray laser interferometry occured in 1997, with a Fresnel bi-mirror interferometer[4]. The short wavelength and the very high brightness of soft x-ray laser (XRL)[5] is an incentive to consider them as promising sources for interferometry experiments.

We present in this paper the first 'in situ' surface diagnostic experiment using an X-W interferometer with an x-ray laser. The aim of this work is to study the evolution of a niobium surface under a strong electric field. A test niobium surface has been chosen on account of its frequent use in superconductive cavities of particle accelerator. This niobium surface sample

---

F. A.: Email: francois.albert@lsai.u-psud.fr; Ph. Z.: Email: philippe.zeitoun@lsai.u-psud.fr

was submitted to a strong electric field in order to measure the morphology defects induced by such a stress. This experiment is crucial because these defects are suspected to be responsible for breakdowns which occurs in superconductive cavities and irremediably damage them.

These cavities are studied to work in new generation particle accelerators with electric fields up to 30 MV/m. But at present time, they are working only under electric field of few MV/m. Further than 5-10 MV/m, induced electrical breakdowns damage the cavities. The mechanisms of such a limitation are not well known. It seems that surface defects and impurities are responsable of the breakdown ignition probably through the appearance of field emission[6]. It has often been suggested that even particulary good quality surface could be modified by a strong electric field and thus, produce preferential electric emission sites. It is this aspect of surface evolution under a strong electric field that we aimed to study. Consequently, the experiment had to be 'in situ' i.e. during the application of high electric field. The interferometric experiment is appropriate for that kind of measurement. But for a surface study under a strong electric field, the wavelength range was limited to X-UV to prevent surface damage due to the laser-surface interaction. The time resolution is also necessary as breakdown occurs in several hundred picoseconds.

In the following table, the main x-ray sources available for this kind of experiment are summarised. In order to provide 'in situ' data, the source needs to be sufficiently bright and brief for single shot recording. The very high number of XRL photons per pulse leads the choice of the source towards the XRL. Thus, the very high brightness (10^{14} W/cm^2/steradian/10^4 BW) of the x-ray laser enables to have a sufficiently high number of coherent photons which can interfere. This insure the good quality of interferograms.

Source	**X-ray laser** **ZN^{20+}**　　　**LSAI**	Harmonic generation Ar　　　　　Saclay	Sincrotron ondulator 　　　　　　ALS
Wavelenght	21.2 nm	~ 20 nm	Tunability
Photon/pulse	**~10^{14}**	10^9	~10-6
Pulse duration	50-80 ps	50 fs	50 ps
Power/pulse	**~ 12 MV**	100 kW	2 kW
Spectral brightness	**10^{16} W/cm^2/steared/10^{-4} BW**	10^{13} W/cm^2/steared/10^{-4} BW	10^8 W/cm^2/steared/10^{-4} BW

Table 1: Main X-ray sources performances. For such an experiment, the relevant characteristics are the X-UV wave length, the pulse duration and the very high brightness. This last is 8 orders of magnitude higher for the XRL than for other souces.

During this experiment, shots performed in fixed conditions without electric field, demonstrated that the surface was kept identical from a shot to another one, owing to the X-UV wavelength. The 80 ps of the pulse was sufficiently short to provide quasi instantaneous image of the surface.

In this work, we will first describe the experimental set-up. Then the results will be analysed by two complementary techniques in order to bring out the global evolution of the surface and to measure this global evolution amplitude.

　　　　　　　　　　　　　　　　　　　　　　　　　　　SRF97D09

2. THE EXPERIMENTAL SET-UP

The x-ray laser is created by the population inversion between the 3p and 3s levels of a neon-like zinc ions immerged in a dense (1/100 solid density) and hot (10 million ^{0}C) plasma. To get this amplifying medium a high power (450J-600ps) IR laser is focused on a 2 cm long zinc slab target. The cylindrical geometry of the optics leads to the production of a plasma column. The amplification of spontaneous emission is maximum in the axis direction. The figure 1 illustrates this geometry.
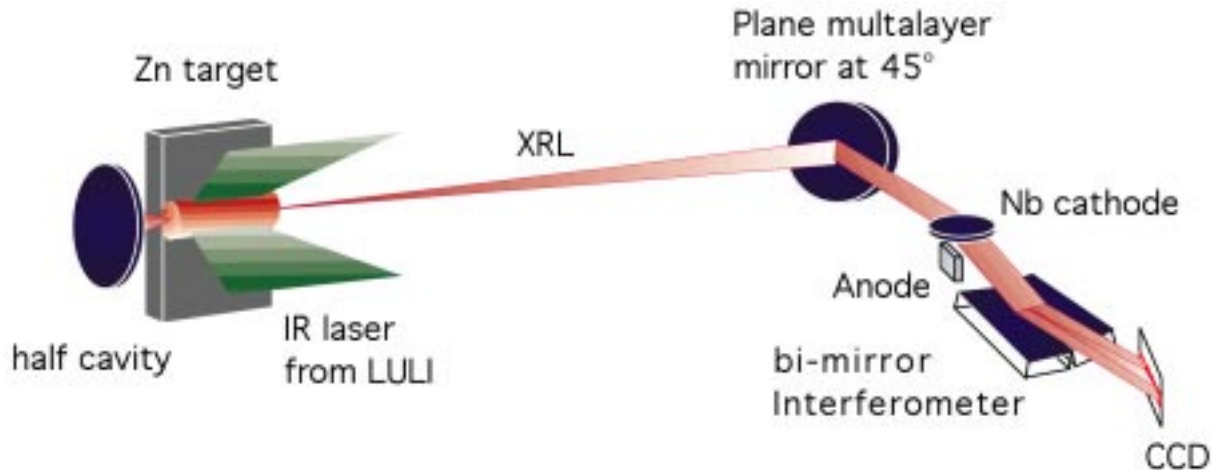
Figure 1: experimental set-up. The high power IR laser is focused on a zinc target. The plasma thus produced generates the x-ray laser. It is send towards the experiment via a 45 ^{0} multilayer mirror. After reflection on the niobium probed sample the beam interfere by superimposition of its two halves owing to the Fresnel bimirror. Interferograms are recorded on a CCD.

A multilayer spherical mirror is used to re-inject one of the two outcoming beams in the amplifying medium. This double-pass amplification leads to a strong domination of stimulated emission. The XRL intensity is multiplied by a factor 80 with regards to the single pass intensity. The brightness is multiplied by a factor of 400 due to the collimation enhancement of the beam. This double pass amplification enables to reach the brightness requiered, without using extra pumping energy.

The x-ray laser beam is then sent towards the interferometer via a flat, 45^0 multilayer mirror. This last is used in order to filter the plasma X-UV background emission, leading to an improvement of the signal to noise ratio.

As shown in figure 2, the flat niobium sample used as a cathode is set under a 5.3^0 grazing incidence. The diameter of the sample is 10 mm and the total surface is enlighted by the x-ray laser. An anode of 200 μm x 6 mm is put in regards to the Nb cathode witn a cathode-anode spacing of 750 μm. The blade shape and the position of the anode has been chosen to create electric field up to 35 MV/m with a power supply of 24 kV. This anode is placed to create an electric field mainly on one half of the probed surface. The other half is used as a reference.

The x-ray laser is then reflected on the Fresnel bi-mirror. This interferometer consists in two grazing incidence mirrors disposed side by side. After reflection, this « ridge roof » geometry leads to a partial superimposition (450 μm) of the two halves of the x-ray laser beam[4]. The generated interferences probe a 450 μm x 10 mm area and are recorded on a CCD. The chip is tilted with a 7.3^0 grazing angle with respect to the XRL axis, in order to provide an apparent magnification (x 6) of the fringe spacing on the recording system.
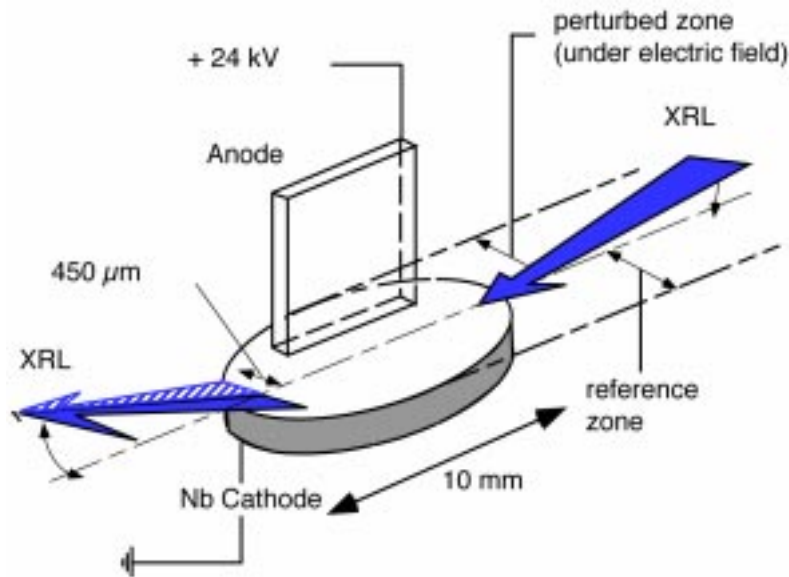
Figure 2: Scheme of the sample set-up. The niobium cathode is used as a grazing incidence mirror. An anode, 750 μm above is used to generates the strong electric f eld on one haf of the sample surface.

3. EXPERIMENTAL RESULTS

An example of interferograms is shown in figure 3, with its characteristic scales. The large difference between vertical and horizontal scales results from the anamorphosis due to the grazing angle geometry of the experiment. For the interference pattern of figure 3 there was no electric field applied to the niobium surface. This is the reference for the measurement of fringe shift under electric field. Fringe shift is due to changes in the surface height under electric field which change the optical path length. A shift of $\lambda/2$ (1 light fringe in place of a dark fringe) corresponds to a height variation of 50.7 nm. So by comparing the interferograms under electric field and the reference pattern, one evidences surface modifications. Another possible cause of change in optical path difference is the variation of refractive index. This may occur with the presence of niobium oxides on the surface. In the present case, the optical path difference due to index variations are smaller than the measurement accuracy -4 nm ($\pm$2 nm) -.Thus we will disregard them.
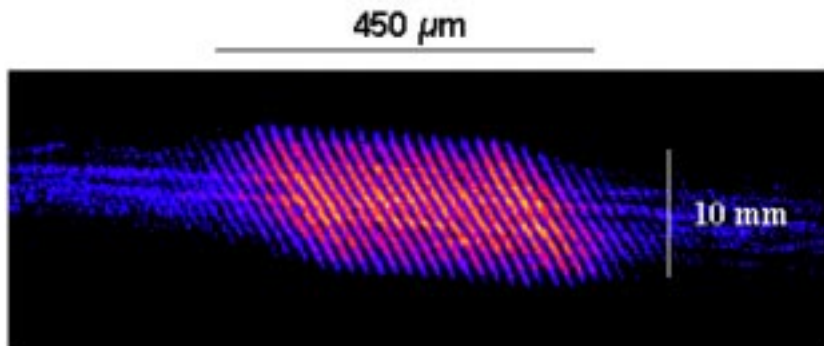
Fig. 3 : Interference pattern of the niobium surface under a 0 MV/m electric field, the characteristic scales are given, the strong anamorphosis is due to the grazing angle geometry of the experiment.

3.1 Interferogram substraction

First we substract intensities, pixel by pixel, between the reference interferogram (Fig.3) and the interferogram recorded inpresence of electric field. Fringe shift make the possible defect zones to clearly appears, as it is shown in figure 4. This simple method is very useful to locate the defects and observe their evolution, because information is not located only in the interferogram but also on the side of it.

a) 9 MV/m

b) 25MV/m

c) 35 MV/m

d) 35 MV/m (20 mn later)
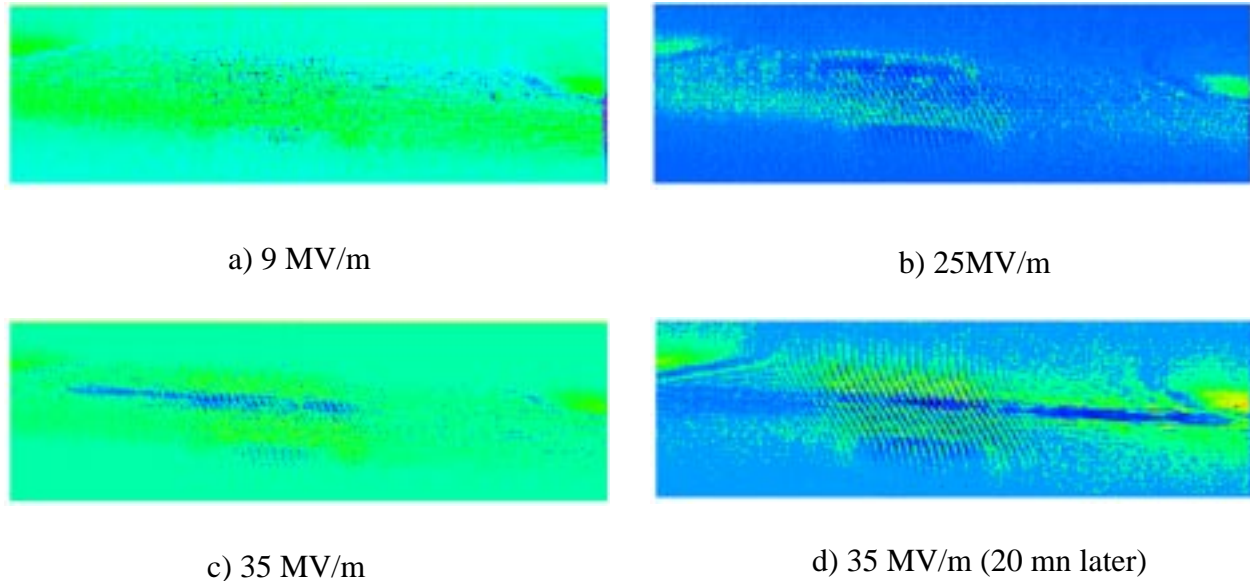
Figure 4: Data treatment based on interferogram substraction. The surface defect appears only for strong electric fields (> 25 MV/m). This analysis has shown that the defect were moving under constant electric field.

In the fourth case presented in figure 4, we see surface modification to appear only for strong electric field. At 9 MV/m the surface is unchanged. The remanent fringes in the bottom image correspond to the anode shadow, not to a defect. At 25 MV/m deformations appear on the top of the image. It is worth noting that we have observed a surface modification before any breakdown. Actually, while increasing the field in order to reach 35 MV/m, a breakdown occured and was detected on a pico-ammeter. This generated a strong modification in an area shifted and larger than for the previous shot. Due to the grazing incidence there is a ratio of 10 between the scales on the different axis, so the shape of the defect visible on the figure 4c) is in fact approximatly circular on the surface, with a diameter of about 300-400 µm.

But the most interesting and surprinsing result is the evidence, 20 minutes later, of the surface deformation evolution under constant electric field. The defect took place 500 µm more on the right of the image. This is quite large in comparison with the 200 µm anode width. At our knowledge, this is the first observation of a breakdown precursor and of the surface defect propagation.

3.2 Hologram reconstruction.

As any interferogram, the ones we obtnained can also be treated as holograms. This enables to compute the wave phase in the sample plane with a reconstruction program. A simulated XRL

wavefront is propagated through the interferogram up to the sample plane. The wave phase thus calculated is proportional to the surface height in each point.

Due to constant calculation artefacts induced by such a reconstruction (limited in distance and spatial frequency planes), it is more convenient to consider the problem in terms of phase variation between the interferograms under field and the reference one, than in terms of absolute phase. As the relevant information is contained only in the fringe pattern, calculations are limited to a zone shown in figure 5.
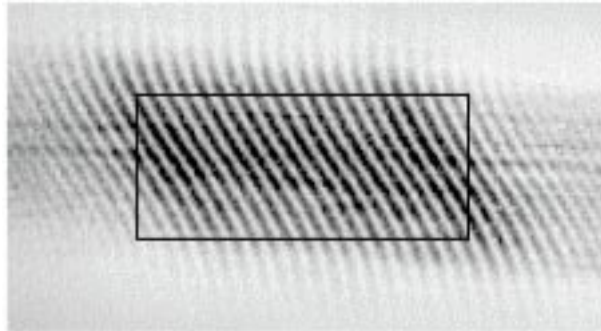
Figure 5: Localisation of the relevant information on the interferogram.
The inner frame shows the area considered for our wave phase calculations.

The important informations are the deformation of the surface related to the discharge and during the next 20 minutes at constant field. The height variation between the two shots before and after the micro-discharge is shown in figure 6a. In figure 6b, the same kind of information is shown between the two shots at 35 MV/m, separated by 20 minutes.

In the first case a), the whole material has moved towards the anode (only positive values), with peaks (white spots) and valleys (black spots). Since the sample was originally polished at optical quality (15Å rms), it appears the electric field has dramatically modified the surface.

After 20 minutes in figure 6b, the whole material has moved again towards the anode, and the differents area enable to measure the amplitude of the deformation change, which is up to 16 nm. This shows that parts of the surface are growing towards the anode and some others are moving back with regards to the average heigh of the sample.

This technique gives quantitative results on a wide area (10 mm x 300 µm). The interferogram substraction gives more qualitative informations on an even larger area. The complementarily of the 2 approaches is necessary to a good understanding of the observed phenomena
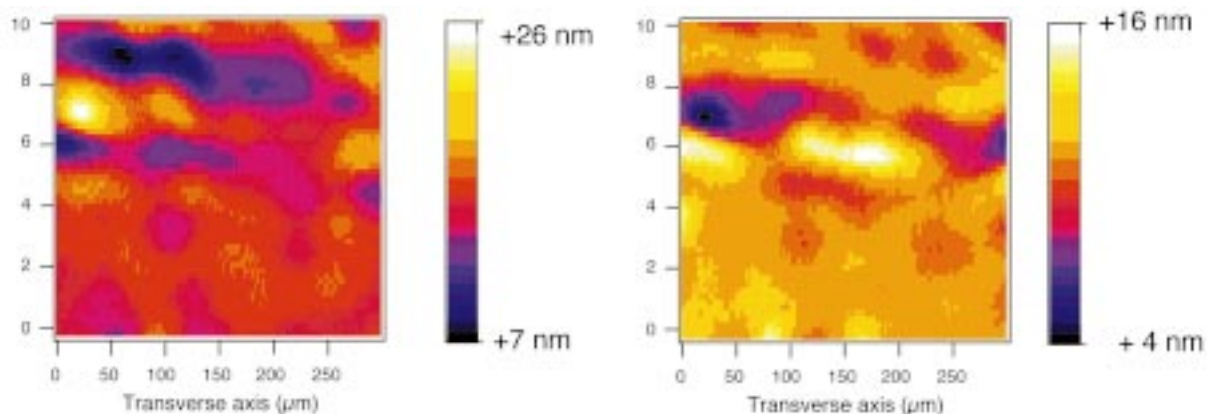
Figure 6: Height variation before and after the micro-discharge a)
and over 20 minute under constant electric f eld b

3.3 Microscope analysis

A complementar analysis has been achieved by different microscopes: atomic force microscope (AFM), scattered electron microscope (SEM) and a phase contrast microscope. These analysis which are usally performed to investigate surfaces after breakdown, here are used to be compared to results from XRL interferometry. The most interesting picture is presented in the next figure.
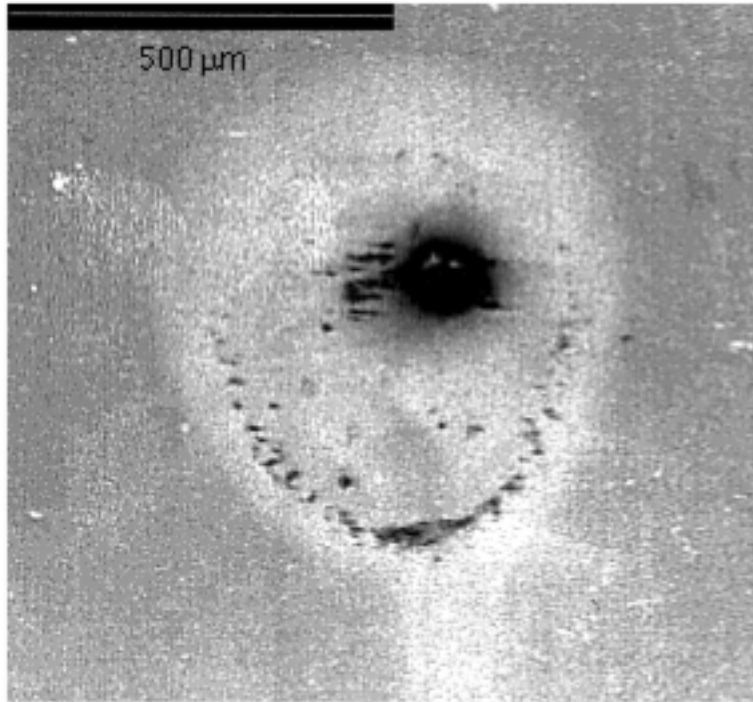
Figure 7: SEM Microscope analysis of the niobium surface. This overview of the breakdown shows the impact in the center and a semi circular structure below. A lighter area shows that the surface density has been modified on a circular shape of ~ 400 μm.

The black spot shape at the center of the SEM image is characteristic of an electrical breakdown. furthermore analysis, wheras only the anode contains iron. The lighter area on center of the SEM image indicates that the surface density has changed. Note that the circular shape of this area of 400 μm in diameter is consistent with the observation done by the X-ray laser interferometer. The black half circle structure on the bottom edge has been analysed by AFM and the height variation is also confirmed. In that case, the structure is purely composed of niobium. On both AFM and phase contraste microscope contaminations from polishing have been found, confirming that the sample was initially not chemically pure, which is known to favorise breakdowns.

CONCLUSIONS

This experiment has been performed to demonstrate the capability of the x-ray laser interferometry in measuring surface deformation. With a fringe visibility of 50%, the resolution achieved by such an instrument is of the order of $\pm \lambda/40$, that is to say ± 2 nm with a 6^0 grazing angle geometry. The data are recorded during 80 ps, leading to time resolution. 'In situ' observation has given the first evidence that surface defects were strongly evoluting under constant electric field.

In further experiments, the work conditions of the sample will be closest door to the conditions in superconductive cavities especially in using ultra high vacuum (10^{-10} instead of 10^{-6} Torr). We will also test the effect of a calibrated surface defect and try to determine the influence of surface stoechiometry. Using UHF electric field and low temperature to reach the superconductive regime, is necessary to be closer to superconductive cavities working conditions.

Through the multiplication of such application experiments, the x-ray laser at 21.2 nm turns to be the prototype of a future « X-W laser facility » aimed to provide high intensity and coherent radiation for application experiments.

AKNOWLEDGEMENTS

REFERENCES

1 L.B. *Da* Silva et al., « Electron density measurement of high density plasmas using Soft X-ray laser interferometry», Phys. Rev. Lett., 74(20), p 3991-3994, 15 May 1995.

2 P. Janglé et al., « Ultraviolet luminescence of CsI and CsCI excited by soft x-ray laser », J. Appl. Phys., 81(5), p2406-2409, I March 1997.

3 LULI: Laboratoire d'Utilisation des Lasers Intenses, Ecole Polytechnique, 91128 Palaiseau cedex, France

4 F. Albert et al., «First interferograms obtained with a X-ray laser by means of a wavefront division interferometer», Opt. Com., to be published,

5 see for instance *X-ray Lasers 1996,* Proceedings of the 5th International Conference on X-ray Lasers, 151, IOP, Lund (Sweden), 1 996.

6 M. Boussoukaya et al., «Low level electron field emission current intensities obtained from niobium samples », Nuclear Instruments and Method in Physics Research A 373, Elsiever Sciences, pl68-174, 1996.

SRF97D09